

---

# A CONSERVATIVE HYBRID PHYSICS-INFORMED NEURAL NETWORK METHOD FOR MAXWELL–AMPÈRE–NERNST–PLANCK EQUATIONS

---

A PREPRINT

Cheng Chang<sup>\*</sup>, Zhouping Xin<sup>†</sup>, Tiejong Zeng<sup>‡</sup>

December 12, 2023

## ABSTRACT

Maxwell–Ampère–Nernst–Planck (MANP) equations were recently proposed to model the dynamics of charged particles. In this study, we enhance a numerical algorithm of this system with deep learning tools. The proposed hybrid algorithm provides an automated means to determine a proper approximation for the dummy variables, which can otherwise only be obtained through massive numerical tests. In addition, the original method is validated for 2-dimensional problems. However, when the spatial dimension is one, the original curl-free relaxation component is inapplicable, and the approximation formula for dummy variables, which works well in a 2-dimensional scenario, fails to provide a reasonable output in the 1-dimensional case. The proposed method can be readily generalised to cases with one spatial dimension. Experiments show numerical stability and good convergence to the steady-state solution obtained from Poisson–Boltzmann type equations in the 1-dimensional case. The experiments conducted in the 2-dimensional case indicate that the proposed method preserves the conservation properties.

**Keywords** Maxwell–Ampère–Nernst–Planck equations · Conservative numerical scheme · Deep learning · Physics-informed neural network

## 1 Introduction

During the past few years, deep learning technologies have flourished in various applications, such as image processing [1], speech recognition [2], and natural language processing [3]. In addition to those high-level tasks which have traditionally thought to require human’s intelligence, deep learning techniques also demonstrate their efficacy in dealing with low-level problems such as partial differential equations (PDEs). Dated back to 1990s, the authors of [4] use the total  $l_2$  error corresponding to the governing equations and boundary conditions at collocation points as the loss function. By minimising it the neural network is trained to fit the equations. In [5], the authors propose more sophisticated formulations in which the initial and boundary conditions are enforced by construction; thus, only the residual for the governing equations need to be included in the training loss. Recently, more algorithms applying deep learning to solve PDEs were proposed. In [6], the authors propose a mesh-free method, and meanwhile provide an efficient approximate algorithm to calculate expressions involving a large number of second-order derivatives, thereby alleviating the curse of dimensionality [7]. Elliptic equations can be solved by optimising the variational problem corresponding to the

<sup>\*</sup>Department of Mathematics & Institute of Mathematical Sciences, The Chinese University of Hong Kong. Email: chengchang@link.cuhk.edu.hk. Address: Room G08, Lady Shaw Building, The Chinese University of Hong Kong, Shatin, N.T., Hong Kong Special Administrative Region, People’s Republic of China

<sup>†</sup>Institute of Mathematical Sciences, The Chinese University of Hong Kong. Email: zpxin@ims.cuhk.edu.hk. Address: Academic Building No. 1, The Chinese University of Hong Kong, Shatin, N.T., Hong Kong Special Administrative Region, People’s Republic of China

<sup>‡</sup>Department of Mathematics, The Chinese University of Hong Kong. Email: zeng@math.cuhk.edu.hk. Address: Room 225, Lady Shaw Building, The Chinese University of Hong Kong, Shatin, N.T., Hong Kong Special Administrative Region, People’s Republic of China

original equations [8]. Building upon these proceeding works, Raissi et al. develop the impactful Physics-informed neural network (PINN), providing two different paradigms for solving PDEs with PINN, i.e. continuous and discrete time model for both the forward and inverse problems [9]. After those cornerstone works, numerous variants on PINN are proposed. To name a few, in [10], in order to tackle the jump discontinuities which is common in the solutions of conservation laws (even when smooth initial conditions are given), the authors propose to approximate the solutions in sub-domains with separate PINNs, then combine them with flux at the sub-domain boundary. In variational PINNs, the authors utilise the weak forms of the residual to train neural networks with some set of test functions (e.g., trigonometric functions or polynomials) [11]. For the weak residual of the PDE, in addition to simple test functions, [12] employ one neural network to fit the solution, whereas the other neural network is used as the test function. As an improvement of VPINN, in [13], the authors investigate several popular PINN variants, then point out that their essential difference is the choice of the test functions in the weak formulations, and propose to use localised test functions to assist the training of the neural network in each sub-domain.

Despite the efficacy of PINNs in solving PDEs, the conventional numerical algorithms are incorporated to remedy some defects in deep learning approaches. In [14], the authors discover that the deep neural networks fit low-frequency features first, which differs from many conventional numerical methods. Considering this, a hybrid method is developed, in which the PINN is trained to obtain a coarse-grained solution first, and then a conventional linear solver is applied to refine the solution [15]. A similar method is proposed in [16], however, in a reverse way, where a conventional multigrid solver is applied first to get the solution in the coarsest few levels and then it comes to the deep neural network to rectify the solution to finer levels. Besides using classical numerical schemes and deep learning at different resolution levels, expecting them to perform well in their respective layers, attempts have been made to merge them more interactively. Studies in this direction usually do not rely entirely on automatic differentiation (AD) [17], but utilise some conventional numerical methods to discretise the domain and approximate differential operators. For example, the discrete-time model of PINN has a similar form to classical Runge–Kutta methods, except that intermediate time-step values are generated with a neural network [9]. Fang utilises well-designed examples to illustrate the faults brought by AD, and then proposes a generalised finite difference-like scheme to replace the AD [18]. Finite-difference (FD) approximations for differential operators are also adopted in [19], whereas the cell size is adaptively shrunk near the boundary such that the neighbouring grid points are guaranteed to be inside the domain of interest. In [20], a neural network approximation with AD is applied in regions where the solution is smooth, whereas a Weighted Essentially Non-oscillatory scheme is adopted in non-smooth regions. In [21], the authors propose a number of second-order accurate numerical differentiation schemes in which the derivative terms are obtained through a combination of AD and FD. In [22], a neural network is used as a corrector for partially unknown physics, and a splitting scheme in time is utilised to tackle two sub-problems; one with the neural network and the other without it. In [23], an auto-encoder is trained to obtain latent variable representations, and then the image gradient (a central-difference scheme) operator is used to approximate the second-order derivatives appearing in the heat equation. Auto-encoder is also utilised in [24] to encode not only the solution field (velocity, pressure in Navier–Stokes equations), but also the domain geometry and boundary condition information. Meanwhile, the PDE residual is calculated with classical finite volume schemes.

One of the reasons why the conventional numerical methods are, in some cases, preferable to deep learning approaches is that the solution is guaranteed to fulfil certain physical properties in carefully designed traditional numerical methods. Taking the Poisson–Nernst–Planck (PNP) equations as an example, this system of equations models the dynamics of the ions under a background electric field, which is affected by the distribution of those ions. The total amount of each species of ions remains constant (provided proper boundary condition, e.g., no flux), while the total energy dissipates as time elapses [25]. When a numerical scheme is carefully designed, these properties can be analytically preserved either conditionally or unconditionally [25, 26, 27]. Some studies have attempted to preserve such kind of physical properties in the context of deep learning. In [28], a special network structure is constructed to constrain the trained network to be symplectic, thus better fitting the phase flow of Hamiltonian systems. In [29], simple physical constraints such as odd and even constraints are guaranteed at specially designed hub layers, and more complicated constraints, such as energy conservation are ensured by a separate corrector network. In addition to the hard constraints imposed on neural network structures, in [30], the authors propose adding soft constraints on physical properties (e.g. mass conservation) to the neural network by introducing a penalty term into the training loss.

In this study, we propose a numerical method which is built upon conventional FD discretisation [31] and introduce a neural network approximator to solve Maxwell–Ampère–Nernst–Planck (MANP) equations [32]. As the original scheme, the proposed hybrid scheme also possesses properties such as mass conservation and positivity preservation. Furthermore, it does not rely on experimental formulas and is more flexible when the problem settings are altered. The remainder of this paper is organised as follows. In Section 2, we give a brief review on MANP equations and the original numerical scheme. In Section 3, we briefly review the general framework of the PINN. We present our proposed hybrid PINN method in Section 4. The numerical experiments are in Section 5

## 2 Maxwell–Ampère–Nernst–Planck equations and its numerical method

Consider the equations on spatial domain  $\Omega \subset \mathbb{R}^d$  and time interval  $[0, T]^1$ :

$$\begin{cases} \frac{\partial c^l}{\partial t} = -\nabla \cdot \mathbf{J}^l, l = 1, 2, \dots, M & (1) \\ \frac{\partial \mathbf{D}}{\partial t} = -\sum_{l=1}^M q^l \mathbf{J}^l + \Theta & (2) \\ \mathbf{J}^l = -(\nabla c^l - \frac{q^l c^l}{\epsilon} \mathbf{D}), l = 1, 2, \dots, M & (3) \\ \nabla \cdot \Theta = 0 & (4) \\ \nabla \times \frac{\mathbf{D}}{\epsilon} = 0 & (5) \end{cases}$$

in which  $l$  is the index for the species of ions,  $c^l : \Omega \times [0, T] \rightarrow \mathbb{R}^+$  is the concentration of the  $l$ -th ions,  $\mathbf{D} : \Omega \times [0, T] \rightarrow \mathbb{R}^d$  is the electric displacement relating to electric potential  $\phi$  via  $\mathbf{D}/\epsilon = -\nabla\phi$ ,  $\epsilon : \Omega \rightarrow \mathbb{R}^+$  is the permittivity,  $q^l \in \mathbb{Z}$  is the valence of the  $l$ -th ions. Differentiate both side of the Poisson's equation  $\nabla \cdot (\epsilon \nabla \phi) = \sum_{l=1}^M q^l c^l + \rho^f$  with regard to time  $t$ , then employ the identity  $\mathbf{D}/\epsilon = -\nabla\phi$  and Equation 1 to obtain that  $\frac{\partial \mathbf{D}}{\partial t} + \sum_{l=1}^M q^l \mathbf{J}^l$  is divergence-free. Representing this quantity with  $\Theta$ , Equations 2 and 4 can be reached [32].

In [31] a standard while effective numerical scheme is proposed. The main idea of [31] is to discretise Equations 1 and 2 with the flux  $\mathbf{J}^l$  reformulated following [26], then solve forward in time. During this process the deviation from Equation 5 is fixed by local curl-free relaxation algorithm. At time  $t = 0$ , the initial electric potential  $\phi^0$  is obtained with the Poisson's equation:

$$-\nabla \cdot (\epsilon \nabla \phi^0) = \sum_{l=1}^M q^l c^{l, \text{init}} + \rho^f, \quad (6)$$

where  $c^{l, \text{init}}$  is the initial distribution of the  $l$ -th ions, and  $\rho^f$  is the fixed charge. Initial electric displacement  $\mathbf{D}^0$  is calculated with a central difference scheme:

$$\frac{D_{i+\frac{1}{2},j}^0}{\epsilon_{i+\frac{1}{2},j}} = \frac{\phi_{i+1,j}^0 - \phi_{i,j}^0}{\Delta x}, \frac{D_{i,j+\frac{1}{2}}^0}{\epsilon_{i,j+\frac{1}{2}}} = \frac{\phi_{i,j+1}^0 - \phi_{i,j}^0}{\Delta y} \quad (7)$$

Equation 1 is discretised with a central difference scheme

$$\frac{c^{l,n+1} - c^{l,n}}{\Delta t} = -\frac{J_{i+\frac{1}{2},j}^{l,n} - J_{i-\frac{1}{2},j}^{l,n}}{\Delta x} - \frac{J_{i,j+\frac{1}{2}}^{l,n} - J_{i,j-\frac{1}{2}}^{l,n}}{\Delta y} \quad (8)$$

where  $J_{i\pm\frac{1}{2},j}^{l,n}$  and  $J_{i,j\pm\frac{1}{2}}^{l,n}$  are numerical approximations of  $x$ - and  $y$ -entries of flux function  $\mathbf{J}^l$  at the  $n$ -th time step

$$J_{i+\frac{1}{2},j}^{l,n} = -\frac{1}{\Delta x} \left( B(\Delta x q^l \frac{D_{i+\frac{1}{2},j}^n}{\epsilon_{i+\frac{1}{2},j}}) - B(-\Delta x q^l \frac{D_{i+\frac{1}{2},j}^n}{\epsilon_{i+\frac{1}{2},j}}) \right), \quad (9)$$

where  $B(x) = \frac{x}{e^x - 1}$ . Similarly for others.

For  $\mathbf{D}$ , an intermediate value (denoted by  $\mathbf{D}^*$ ) is first calculated with the discretised Maxwell–Ampère equations 2 and 3:

<sup>1</sup>For simplicity, we omit those physics constant coefficients and mean field approximation correction terms, which are of little importance for the presentation of the proposed numerical scheme.

$$\frac{\mathbf{D}^* - \mathbf{D}^n}{\Delta t} = - \sum_{l=1}^M q^l \mathbf{J}^{l,n} + \Theta^n, \quad (10)$$

where  $\Theta^n = \frac{\mathbf{D}^n - \mathbf{D}^{n-1}}{\Delta t} + \sum_{l=1}^M \frac{q^l}{2\kappa^2} \mathbf{J}^{l,n-1}$  has been proven as the best approximation for  $\Theta^n$  through massive numerical tests [32]. Because the value of  $\Theta$  is an approximation, the value of  $\mathbf{D}^*$  is not the true value for the next time step. This may violate Equation 5. Thus, starting from  $\mathbf{D}^*$ , an iterative constrained optimisation algorithm is performed to restore the correct value of  $\mathbf{D}^{n+1}$ :

$$\mathbf{D}^{n+1} = \arg \min_{\mathbf{D}} \int_{\Omega} \frac{\|\mathbf{D}\|^2}{\epsilon} \text{ s.t. } \nabla \cdot \mathbf{D} = \sum_{l=1}^M q^l c^{l,n+1} + \rho^f. \quad (11)$$

The minimiser of Equation 11 satisfies  $\mathbf{D} + \epsilon \nabla \phi = 0$  for some  $\phi$  by Lagrange multiplier and calculus of variation [33], which means Equation 5 is satisfied.

### 3 Deep neural network and PINN

Consider the PDE

$$\begin{aligned} \mathcal{N}u(\mathbf{x}, t) &= f(\mathbf{x}, t), \mathbf{x} \in \Omega \subset \mathbb{R}^n, t \in [0, T] \\ \mathcal{B}u(\mathbf{x}, t) &= g(\mathbf{x}, t), \mathbf{x} \in \partial\Omega, t \in [0, T] \\ u(\mathbf{x}, 0) &= u_0(\mathbf{x}), \mathbf{x} \in \Omega \end{aligned} \quad (12)$$

where  $u$  is the unknown solution function,  $\mathcal{N}$  is a (probably nonlinear) differential operator,  $f$  is a known inhomogeneous term,  $g$  is a known function defining the solution values at the boundary  $\partial\Omega$ ,  $u_0$  is a known initial condition. The analytic solution is usually difficult to find even for a seemingly simple form of  $\mathcal{N}$ ; thus, the numerical methods for PDEs are then pursued. PINN [9] has gained much attention in the community of scientific computing due to its portability and promising accuracy. The essence of PINN is the utilisation of a deep neural network as the approximator to fit the unknown solution function, similar to the polynomials employed in finite element methods. The basic building block of a deep neural network is called the layer, usually composed of an affine transformation and a nonlinear activation function. Mathematically, a layer  $l_i : \mathbb{R}^{n_i} \rightarrow \mathbb{R}^{n_{i+1}}$ ,  $i = 1, 2, \dots, L$  can be written as

$$l_i(\mathbf{x}) = \sigma_i(\mathbf{W}_i \mathbf{x} + \mathbf{b}_i), i = 1, 2, \dots, L, \quad (13)$$

where  $\mathbf{W}_i \in \mathbb{R}^{n_{i+1} \times n_i}$ ,  $\mathbf{b}_i \in \mathbb{R}^{n_{i+1}}$ , and  $\sigma_i : \mathbb{R}^{n_{i+1}} \rightarrow \mathbb{R}^{n_{i+1}}$  is a nonlinear (usually element-wise) activation function. The whole deep neural network can be written as

$$\tilde{u}(\mathbf{x}; \boldsymbol{\theta}) = l_L \circ l_{L-1} \circ \dots \circ l_1(\mathbf{x}), \quad (14)$$

where  $\circ$  denotes the function composition, and  $\boldsymbol{\theta} := \{\mathbf{W}_i, \mathbf{b}_i\}_{i=1}^L$  is the collection of the network parameters. The variable  $\mathbf{x}$  is the input to the neural network. In the settings of evolution equations, the input includes both the spatial variable and time, which can be packed to form one input vector (the continuous-time model). In the remainder of this section, we abuse the variable  $\mathbf{x}$  to solely denote the spatial variable, thus the input to the network should be written as  $(\mathbf{x}, t)$ .

To train the neural network means to optimise some loss function with regard to the network parameter  $\{\mathbf{W}_i, \mathbf{b}_i\}_{i=1}^L$  utilising some optimisers, such as Stochastic Gradient Descent [34] or ADAM [35]. In the PINN [9], the loss function contains the information of the governing equation (see Equation 12) at collocation points  $\{(\mathbf{x}_i, t_i)\}_{i=1}^{N_{eq}} \subset \Omega \times [0, T]$  and paired data (usually obtained from initial and boundary conditions)  $\{(\mathbf{x}_{D,i}, t_{D,i}), u_{D,i}\}_{i=1}^N$ :

$$\mathcal{L} = \frac{1}{N_{eq}} \sum_{i=1}^{N_{eq}} (\mathcal{N}\tilde{u}(\mathbf{x}_i, t_i) - f(\mathbf{x}_i, t_i))^2 + \frac{1}{N} \sum_{i=1}^N (\tilde{u}(\mathbf{x}_{D,i}, t_{D,i}) - u_{D,i})^2 \quad (15)$$

The differentiation operations appearing in  $\mathcal{N}$  and  $\mathcal{B}$  can be handled with AD [17].

## 4 Hybrid PINN

As remarkable as the original numerical method is, some improvements can still be achieved. Firstly, the relaxation algorithm to correct the intermediate  $\mathbf{D}^*$  requires changes in one cell to be compensated for in another cell; thus, it is inapplicable in the 1-dimensional case. Section 5.1 demonstrates that the same formula does not work for the same system in the 1-dimensional case. Therefore, a method to obtain an accurate intermediate value for the electric displacement is required. Secondly, it is far from obvious how to incorporate boundary condition involving  $\mathbf{D}$  in the original conventional numerical method. For example, a common boundary condition for this system is the Neumann boundary condition

$$\frac{\partial \phi}{\partial \mathbf{n}}(\mathbf{x}) = g(\mathbf{x}), \mathbf{x} \in \partial\Omega, \quad (16)$$

where  $\mathbf{n}$  is the outward normal vector and  $g$  is known. From the identity  $\mathbf{D}/\epsilon = -\nabla\phi$ , this boundary condition can be expressed in terms of  $\mathbf{D}$ :

$$-\frac{\mathbf{D}}{\epsilon} \cdot \mathbf{n} = g. \quad (17)$$

Thirdly, the variable  $\Theta$ , coming with the introduction of the novel Maxwell–Ampère equation (Equations 2 and 3), brings an additional degree of freedom. There is no theoretical result for the value that should be chosen, except that it is divergence-free (see Equation 4). In [32, 31], the value is selected via heuristics. They provide three options for  $\Theta$ , and in their numerical tests the second one  $\Theta^n = \frac{\mathbf{D}^n - \mathbf{D}^{n-1}}{\Delta t} + \sum_{l=1}^M q^l \mathbf{J}^{l,n-1}$  is proven to be the best. It is curious because the third choice  $\Theta^n = \frac{3}{2}(\frac{\mathbf{D}^n - \mathbf{D}^{n-1}}{\Delta t} + \sum_{l=1}^M q^l \mathbf{J}^{l,n-1}) - \frac{1}{2}(\frac{\mathbf{D}^{n-1} - \mathbf{D}^{n-2}}{\Delta t} + \sum_{l=1}^M q^l \mathbf{J}^{l,n-2})$  indeed gives higher order of accuracy. This suggests that figuring out principled guidance for approximations to this variable might be difficult. Clearly, considerable efforts have been invested in determining a delicate formula which will work practically. To make things worse, this formula is not universal, meaning that it merely applies to this particular system, and might be completely useless when the equations are further modified owing to advances in physics.

To tackle the issues, we propose to use a neural network to calculate the values of the variable  $\Theta$ . This section presents our proposed hybrid scheme for solving MANP equations, analyses its conservative properties, and describes situations in 1-dimensional problems in details.

### 4.1 Approximation to $\Theta$ through neural network

Unlike vanilla PINN, for  $\Theta$ , we have neither paired data nor explicit governing physical laws; hence, a novel approach to design the loss function is required. According to Equation 10,  $\Theta$  and  $\mathbf{D}$  are closely related; thus, we propose controlling the value of  $\mathbf{D}$  to indirectly guide the training of the neural network. For  $\mathbf{D}$ , there are governing Equations 2 and 3. However, because many variables are involved, numerical errors from these variables may accumulate. In addition, it slows down the training because the loss value and its partial derivatives with regard to every network parameter must be calculated in each training loop. To improve efficiency, we apply Equation 5 to design the loss function. The straightforward formulation is as follows:

$$\mathcal{L}_{PI}(t) = \frac{1}{N} \sum_{i=1}^N \left( \frac{\partial}{\partial x} \frac{D^{(2)}}{\epsilon}(x_i, y_i, t) - \frac{\partial}{\partial y} \frac{D^{(1)}}{\epsilon}(x_i, y_i, t) \right)^2, \quad (18)$$

or an alternative loss design adopting Lagrange multiplier to eliminate the derivative term [33]:

$$\mathcal{L}'_{PI}(t) = \frac{1}{N} \sum_{i=1}^N \left( \left( \frac{D^{(1)}}{\epsilon}(x_i, y_i, t) \right)^2 + \left( \frac{D^{(2)}}{\epsilon}(x_i, y_i, t) \right)^2 \right) \quad (19)$$

where  $D^{(1)}$  and  $D^{(2)}$  are  $x$ - and  $y$ -entry of the vector field  $\mathbf{D}$ , respectively,  $\{(x_i, y_i)\}_{i=1}^N$  are the spatial locations used in training, and  $t$  is the current time step. Equation 19 does not contain derivative terms; therefore, it is more numerically stable. In the numerical experiments, we find that Equation 19 gives better results.

*Remark.* To be rigorous, the minimiser of Equation 19 is not the solution satisfying  $\frac{D}{\epsilon} = -\nabla\phi$  and the  $\nabla \cdot \mathbf{D} = \sum_{l=1}^M q^l c^l + \rho^f$ . The true solution is the constrained minimiser under the condition  $\nabla \cdot \mathbf{D} = \sum_{l=1}^M q^l c^l + \rho^f$ . From Equation 10, we can see that given  $\Theta$  is divergence-free in the discrete sense, and the current  $\mathbf{D}$  satisfies this constraint, the updated  $\mathbf{D}^*$  will do so. It will be shown that in our proposed method, the divergence-free condition can be automatically and analytically guaranteed; thus, we can safely discard the constraint, and perform unconstrained optimisation, for which many techniques exist in deep learning contexts.

As mentioned before,  $\Theta$  and  $\mathbf{D}$  are closely related, we apply the numerical value of the previous time step as the input of the neural network [36, 37]. Inspired by Theorem 3.1 in [38], we train it to fit a hidden scalar field  $\tilde{u}(x, y, t)$  then obtain the entries  $(\Theta^{(1)}, \Theta^{(2)})$  of the target  $\Theta$  through

$$\begin{aligned}\Theta^{(1)}(x_i, y_i, t) &= \frac{\tilde{u}(x_i, y_{i+1}, t) - \tilde{u}(x_i, y_i, t)}{y_{i+1} - y_i} \\ \Theta^{(2)}(x_i, y_i, t) &= -\frac{\tilde{u}(x_{i+1}, y_i, t) - \tilde{u}(x_i, y_i, t)}{x_{i+1} - x_i}.\end{aligned}\tag{20}$$

Using this formulation, the divergence-free condition is satisfied automatically in the discrete sense. Thus, we only need to minimise  $\mathcal{L}'_{PI}$  (Equation 19) during training the neural network.

Because deep learning is an optimisation-based numerical approximation method, it is highly flexible to implement almost any boundary condition, as a penalty term. Take the Neumann boundary condition (Equation 17) as an example, the penalty term can be written as:

$$\mathcal{L}_{BC}(t) = \frac{1}{N_{BC}} \sum_{i=1}^{N_{BC}} \left( -\frac{\mathbf{D}(x_i, y_i, t)}{\epsilon} \cdot \mathbf{n} + g(x_i, y_i, t) \right)^2,\tag{21}$$

where  $\{x_i, y_i\}_{i=1}^{N_{BC}}$  are the grid points at the boundary. In practice, because the values of  $\Theta^{(1)}$  and  $\Theta^{(2)}$  should not vary too much in a single discrete cell, to avoid overfitting and instability, we add a regularisation term:

$$\begin{aligned}\mathcal{R}(t) &= \int_{\Omega} \|\nabla\Theta^{(1)}(x, y, t)\|_2^2 + \|\nabla\Theta^{(2)}(x, y, t)\|_2^2 dx dy. \\ &\approx \Delta_x \Delta_y \sum_{i=1}^N \left( \|\nabla\Theta^{(1)}(x_i, y_i, t)\|_2^2 + \|\nabla\Theta^{(2)}(x_i, y_i, t)\|_2^2 \right).\end{aligned}\tag{22}$$

The final loss function for the neural network training is:

$$\mathcal{L}(t) = \mathcal{L}'_{PI}(t) + \lambda_{BC}\mathcal{L}_{BC}(t) + \lambda_R\mathcal{R}(t),\tag{23}$$

where  $\lambda_{BC}$  and  $\lambda_R$  are hyper-parameters.

During training, at each time step  $t_i$ , we update the network parameters until the loss function value  $\mathcal{L}(t_i)$  is small enough or a preset training loop threshold is reached.

## 4.2 Analysis of conservative properties

This section analyses the conservation properties of the proposed method: conservation of total mass and preservation of ion concentration positivity. Although a neural network replaces the concrete formula for  $\Theta$ , which introduces stochasticity (e.g., during initialisation and training), the conservation properties are retained, which is different from vanilla pure end-to-end PINN. Such conservation properties are generally difficult to ensure in vanilla PINN. In situations where the network is perfectly trained and converges to the true solution exactly we are certain that these properties are possessed by the numerical solutions given by the neural network. However, in most cases, deep learning practitioners do not have this guarantee. In the proposed method, these conservation properties still hold even if approximation errors are present (e.g. owing to insufficient training).

Theorem 3.1 of [31] establishes the mass conservation property through summing up both sides of Equation 8 over the entire spatial domain. In our method, the values of  $\mathbf{J}$  might be different, because the values given by the neural network

at different training stages affect the value of  $\mathbf{D}$  and, consequently the values of  $\mathbf{J}$ . However, the mass is still conserved because all these  $\mathbf{J}$  cancel provided a periodic boundary condition.

The mass positivity of the original algorithm is proven in Theorem 3.2 of [31]. They first flatten the 2D array containing the ion concentration values at grid points to be Vector  $c^{n,l}$ , then construct Matrix  $\mathcal{L}$  such that  $\mathcal{L}c^{n+1,l} = c^{n,l}$ . The particular matrix entry values obtained in our hybrid method could be different, but this matrix remains strictly diagonally dominant (thus invertible), with positive diagonal entries and negative off-diagonal entries. According to Gershgorin's circle theorem, all eigenvalues have positive real parts; thus, it is an M-matrix. According to statement  $F_{15}$  in [39], its inverse has no negative entries; thus, this transformation preserves positivity.

### 4.3 Generalisation to 1-dimensional problems

Generalising this particular numerical scheme to 1-dimensional problems is not trivial. The first problem is with the empirical equation for the variable  $\Theta$ . Because this expression is obtained from extensive experiments in a 2-dimensional setting, its transfer to 1-dimensional cases remains unclear. We will demonstrate that in 1-dimensional problems, neither directly adapting the formula of  $\Theta$  in the 2-dimensional case, nor simply setting it as 0 will work in numerical experiments. The other reason accounting for the failure of the original algorithm in 1-dimensional problems is that the formula is an approximation for correct  $\Theta$  values. However, this approximation could be inaccurate. To fix possible error caused by this imperfect approximation of  $\Theta$ , in [32, 31], the authors apply a local curl-free relaxation algorithm to correct it. This procedure is simple yet effective in 2-dimensional problems, but in 1-dimensional cases, this algorithm is inapplicable, because once we update the electric displacement in one cell, there is no cell to compensate for it to restore the constraint in Equation 11. The proposed hybrid scheme provides an efficient means to adaptively calculate the proper values for  $\Theta$  in different settings via neural network training, an automatic and user-transparent optimisation process.

Here we describe the proposed method in a 1-dimensional case. The PNP system in a 1-dimensional space is:

$$\begin{cases} \frac{\partial c^l}{\partial t} = -\frac{\partial J^l}{\partial x}, l = 1, 2, \dots, M & (24) \\ J^l = -\left(\frac{\partial c^l}{\partial x} + q^l c^l \frac{\partial \phi}{\partial x}\right), l = 1, 2, \dots, M & (25) \\ \epsilon_0^2 \frac{\partial^2 \phi}{\partial x^2} = -\rho^f - \sum_{l=1}^M q^l c^l, & (26) \end{cases}$$

where  $\epsilon_0$  is a constant. Following the derivation of [32], we take the time-derivative of both sides of Equation 26, plugging in Equation 24, and using  $\Theta$  to represent  $\epsilon_0^2 \frac{\partial}{\partial t} \frac{\partial \phi}{\partial x} - \sum_{l=1}^M q^l J^l$ , the Maxwell–Ampère equation is:

$$\begin{cases} \epsilon_0^2 \frac{\partial}{\partial t} \frac{\partial \phi}{\partial x} = \Theta + \sum_{l=1}^M q^l J^l & (27) \\ \frac{\partial \Theta}{\partial x} = 0. & (28) \end{cases}$$

Following [40], we consider the spatial domain  $[-1, 1]$ . For ionic flux  $J^l$ 's, no flux boundary condition is applied:

$$J^l(-1) = J^l(1) = 0, l = 1, 2, \dots, M, \quad (29)$$

while a Robin-type boundary condition is applied for electric potential  $\phi$ :

$$\begin{cases} \phi(1) + \eta \frac{\partial \phi}{\partial x}(1) = \phi_0(1) & (30) \end{cases}$$

$$\begin{cases} \phi(-1) - \eta \frac{\partial \phi}{\partial x}(-1) = \phi_0(-1), & (31) \end{cases}$$

where  $\eta$ ,  $\phi_0(1)$  and  $\phi_0(-1)$  are constants.

The original numerical scheme solves the MANP equations for  $c^l$ ,  $J^l$  and  $\frac{\partial\phi}{\partial x}$ . Similar to 2-dimensional case, if the value of  $\Theta$  is not correctly selected, the resulting  $\frac{\partial\phi}{\partial x}$  may not corresponding to an existing  $\phi$ , because the Robin-type boundary conditions for  $\phi$  at the right and left ends could contradict. Thus, a loss function reflecting such contradiction should be designed. Considering the difference between both sides of Equations 30 and 31, we obtain:

$$\phi(1) - \phi(-1) + \eta\left(\frac{\partial\phi}{\partial x}(1) + \frac{\partial\phi}{\partial x}(-1)\right) - (\phi_0(1) - \phi_0(-1)) = 0. \quad (32)$$

After  $\frac{\partial\phi}{\partial x}$  is calculated, we use the values of  $\frac{\partial\phi}{\partial x}$  and rectangular rules of numerical integration to approximate  $\phi(1) - \phi(-1)$ :

$$\phi(1) - \phi(-1) = \int_{-1}^1 \frac{\partial\phi}{\partial x}(x)dx \approx \sum_{i=1}^m \frac{\partial\phi}{\partial x}(x_i), \quad (33)$$

where  $-1 = x_1 < x_2 < \dots < x_m$  are the grid points used for numerical integration, and  $m$  is the total number of grid points.

We can write out the loss function as a squared error:

$$\mathcal{L}_{1d} = \left( \sum_{i=1}^m \frac{\partial\phi}{\partial x}(x_i) + \eta\left(\frac{\partial\phi}{\partial x}(1) + \frac{\partial\phi}{\partial x}(-1)\right) - (\phi_0(1) - \phi_0(-1)) \right)^2. \quad (34)$$

Considering that this loss function itself takes the boundary condition into account, and the output of the network is a scalar, we simply discard the loss for the boundary (Equation 21) and the regularisation term (Equation 22).

## 5 Numerical experiments

### 5.1 Steady-state solution in 1-dimensional space

This section presents the numerical results of our proposed method and validate it through its convergence to the steady-state solution as  $t \rightarrow \infty$  following [25]. The steady-state solution is calculated with the method provided by Lee et al [40]. We also compare with the experimental formulas for  $\Theta$  from the original method (together with a variant), which have been proven effective in 2-dimensional cases:

$$\Theta^n = 0, \quad (35)$$

$$\Theta^n = \epsilon_0^2 \frac{\frac{\partial\phi^n}{\partial x} - \frac{\partial\phi^{n-1}}{\partial x}}{\Delta t} - \sum_{l=1}^M q^l J^{l,n-1}, \quad (36)$$

$$\Theta^n = \epsilon_0^2 \frac{\frac{\partial\phi^n}{\partial x} - \frac{\partial\phi^{n-1}}{\partial x}}{\Delta t} - \sum_{l=1}^M q^l J^{l,n}, \quad (37)$$

where  $\Delta t$  is the time step interval, and the superscript  $n$  refers to the index for the time step.

The frame of the numerical scheme is a straightforward generalisation from the original 2-dimensional numerical method. Assume  $\rho^f = 0$  and  $\epsilon_0 = 2^{-2}$ , we first initialise  $\phi^0$  and  $\frac{\partial\phi^0}{\partial x}$  such that they satisfy the Poisson's equation (Equation 26). Numerical values of  $c^l$ 's and  $\frac{\partial\phi}{\partial x}$  are updated for each time step. After  $\frac{\partial\phi}{\partial x}$  is solved, we solve for  $\phi$  according to  $\frac{\partial\phi}{\partial x}$  and the boundary condition at the left end utilising Euler forward ordinary differential equation solver.

Figure 1 illustrates the convergence behaviour of the numerical solutions over time. Simply setting  $\Theta$  to be 0 will not give the correct solution. The direct generalisation of the formula for  $\Theta$  in 2-dimensional cases (Equation 36) exhibits numerical instability in the 1-dimensional problem. When a variant (Equation 37) is applied, the numerical scheme fails to update the solution correctly over time. The solutions at different time steps are identical. By contrast, the solution calculated with the proposed method gradually converges to the steady-state solution.



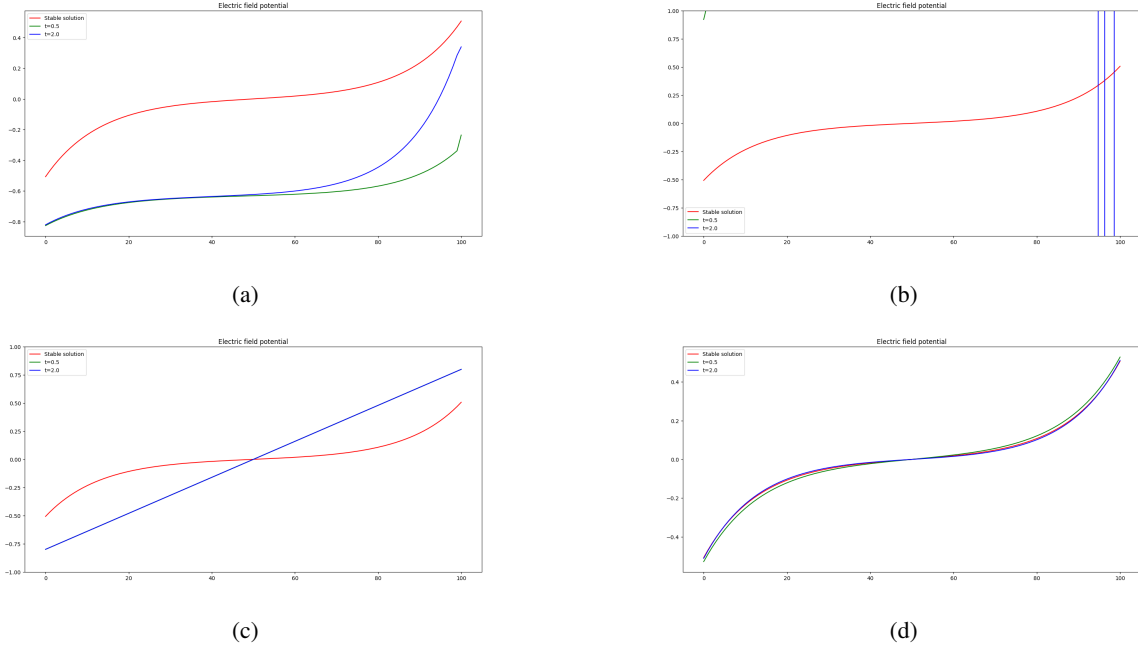


Figure 1: Electric potential  $\phi$  at different time steps. (a)  $\Theta$  is set to be 0; (b)  $\Theta$  is calculated with Equation 36; (c)  $\Theta$  is calculated with Equation 37, the solution at  $t = 0.5$  and  $t = 2.0$  are overlapped ; (d)  $\Theta$  is approximated by a neural network (ours)

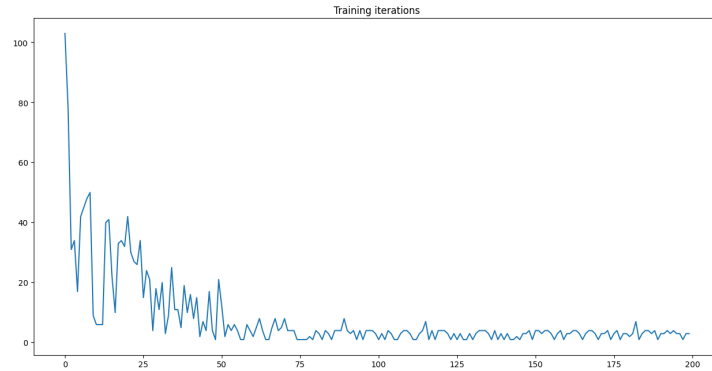


Figure 2: Training iterations required to reach a loss less than  $10^{-8}$

Figure 2 shows the training iterations that the neural network required to optimise the loss value to less than  $10^{-8}$ . Although the number of iterations is large at the beginning of the training, it drops quickly as the time step advances.

There might be an argument that, in this simple problem, the correct optimiser of the loss function can be found analytically without the assistance of a neural network. However, this depends on the discretisation methods employed for the PDE and the numerical integration schemes applied. This may not be the case if a more sophisticated numerical method is adopted. Furthermore, this approach can be immediately applied to another PDE system in which a dummy variable providing an extra degree of freedom without a clear physical meaning is present. Researchers need not conduct extensive numerical tests to determine a well-behaved approximation formula. A correction algorithm is not required to augment the numerical scheme to avoid error accumulation.

Table 1: Running time

Spatial resolution	Ours	Original
$50 \times 50$	1m41.5s	1m49.7s
$100 \times 100$	6m55.2s	10m46.7s

## 5.2 Efficiency analysis

In the original work the local curl-free algorithm is performed cell-by-cell [32, 31]. This implementation is not suitable for parallelisation. We propose calculating the update step sizes for the all cells at once, organising them as matrices, and applying the updates to the whole domain. Although this trade a little accuracy for the efficiency, our proposed method still achieves higher accuracy (see Section 5.3), and meanwhile, the computation time is greatly reduced. Table 1 shows the running time of our method and the original method in [32, 31], both computing 100 time steps from  $t = 0$  to  $t = 0.5$ . The data is measured on an Intel(R) Core(TM) i9-13900HX CPU (no CUDA [41] is utilised for the neural network). It can be observed that even our method includes the overhead of neural network training and inference, with the accelerated local curl-free algorithm, it is still faster, and the edge is larger when the grid is finer. Note that the proposed method is an integrated process including both formula discovery and numerically solving the system, but when running the original method, a well-tested formula to approximate  $\Theta$  found in [32, 31] is already given.

## 5.3 Analytic tests

Consider the domain  $\Omega = [-1, 1] \times [-1, 1]$ , and  $t \in [0, 0.5]$ . Let  $q^1 = +1$ ,  $q^2 = -1$ , and  $\epsilon = 1$ , we assume the exact solution of the system is:

$$\begin{cases} \phi_{true}(\mathbf{x}, t) = \frac{1}{2} \|\mathbf{x}\|_2^2 e^{-t} & (38) \\ c_{true}^1 = e^{-\phi} & (39) \\ c_{true}^2 = e^{\phi} & (40) \\ \mathbf{D}_{true} = -\epsilon \nabla \phi_{true}. & (41) \end{cases}$$

The system is then adapted to fit the exact solution above:

$$\begin{cases} \frac{\partial c^l}{\partial t} = -\nabla \cdot \mathbf{J}^l + f_l, l = 1, 2 & (42) \\ \frac{\partial \mathbf{D}}{\partial t} = -\sum_{l=1}^2 q^l \mathbf{J}^l + \Theta + \mathbf{h} & (43) \\ \mathbf{J}^l = -(\nabla c^l - \frac{q^l c^l}{\epsilon} \mathbf{D}), l = 1, 2, & (44) \end{cases}$$

where  $f_l$ 's are calculated through the exact solution, and  $\mathbf{h}$  is selected to be:

$$\mathbf{h} = \begin{pmatrix} x_1 - x_2 \\ x_2 - x_1 \end{pmatrix} e^{-t}, \quad (45)$$

so that  $\Theta$  is divergence-free (Equation 4). For the  $c^l$ 's, we apply periodic boundary condition, and for  $\mathbf{D}$  we apply boundary condition in the Equation 17, which is the Neumann boundary condition for the electric potential  $\phi$ . The right-hand side of the Equation 17 is obtained from the exact solutions. Suppose the solution given by the numerical algorithm are  $c_{numerical}^l$ 's and  $\mathbf{D}_{numerical}$ , the error of time  $t$  is then calculated via:

$$E_{c^l}(t) = \sqrt{\frac{1}{N} \sum_{i=1}^N (c_{numerical}^l(x_i, y_i, t) - c_{true}^l(x_i, y_i, t))^2} \quad (46)$$

$$E_D(t) = \frac{1}{N} \sum_{i=1}^N \|D_{numerical}(x_i, y_i, t) - D_{true}(x_i, y_i, t)\|_2. \quad (47)$$

We conduct several experiments with different resolutions, and record the error at each time step. In all experiments in this section and Section 5.4, the acceleration method proposed in Section 5.2 is imposed on our method, while the original local curl-free algorithm is used in the original method as a baseline. The error of  $c^1$ ,  $c^2$  and  $D$  are shown in Figure 3.

From the figure, it is clear that although our method shows comparable accuracy at the beginning, as time evolves, the error of our method still keeps constant or declines, while that of the original method inclines. This phenomena can be observed in both  $c^l$ 's and  $D$ , and is more significant in  $D$ .

## 5.4 Electrostatics in 2-dimensional space

The spatial domain is  $\Omega = [-1, 1] \times [-1, 1]$ , and the terminal time  $T = 0.5$ . The cell size  $\Delta x = \Delta y = 0.04$ , and  $\Delta t = 0.0005$ . We assume that the solute is a binary ionic compound with the valence of the cations and anions being +1 and -1, respectively. The compound is assumed to be fully ionised in the solvent, and the resultant ions can freely move in the solvent, under the effects of both themselves and fixed charges in the solvent. The initial concentrations of both kinds of ions are 1 throughout the entire domain.  $\epsilon$  is assumed to be 1. The fixed charges are described by the formula:

$$\rho^f = \begin{cases} 1, & x \in \{(x - 0.5)^2 + y^2 \leq 0.09\} \\ -1, & x \in \{(x + 0.5)^2 + y^2 \leq 0.09\} \\ 0, & \text{otherwise} \end{cases} \quad (48)$$

The loss values of the neural network over time is shown in Figure 4. A good convergence of the neural network is indicated by the stable downward trend of the loss values. In Figure 5, the number of iterations of the local curl-free relaxation algorithm [32, 31] is presented. The algorithm stops when the change of the objective function (Equation 11) value is less than  $10^{-5}$ . Although the number of iterations is large at the very beginning, it drops sharply as the training progresses. It remains 1 since the initial time step (at least one iteration must be executed per time step to calculate the change of the objective function), meaning that the neural network fit the appropriate value well, so that no further correction is required.

The conservations of total mass of ions can be observed in Figure 6. From Figure 7, it can be seen that the positivity of ion concentrations is preserved. Figure 8 illustrates the evolution of the free energy of the system over time. Figure 9 presents the snapshots of the numerical results at different time steps. A converging trend towards opposite charges can be observed from the ion concentration maps. At the borders of the fixed charges there is large electric displacement, and it fades as free ions move.

## 6 Conclusions

This study proposes a hybrid numerical method combining conventional methods and deep learning approaches to solve the MANP equations. A deep neural network is employed to improve the conventional numerical scheme. The resulting hybrid method combines the strengths of both conventional and deep learning methods. First, it preserves the conservation properties of the MANP equations with particular boundary conditions, including the conservation of the total mass of ions and the positivity of the ion concentrations. Second, owing to the flexibility and universal applicability of deep learning, the proposed method exhibits good portability to different problem settings. Numerical experiments on both 1-dimensional and 2-dimensional cases are conducted to validate the method. They demonstrate the generalisation capability of the proposed method as well as the preservation of conservation properties.

## References

- [1] Christian Ledig, Lucas Theis, Ferenc Huszar, Jose Caballero, Andrew Cunningham, Alejandro Acosta, Andrew Aitken, Alykhan Tejani, Johannes Totz, Zehan Wang, and Wenzhe Shi. Photo-realistic single image super-resolution using a generative adversarial network. In *The IEEE Conference on Computer Vision and Pattern Recognition (CVPR)*, July 2017.

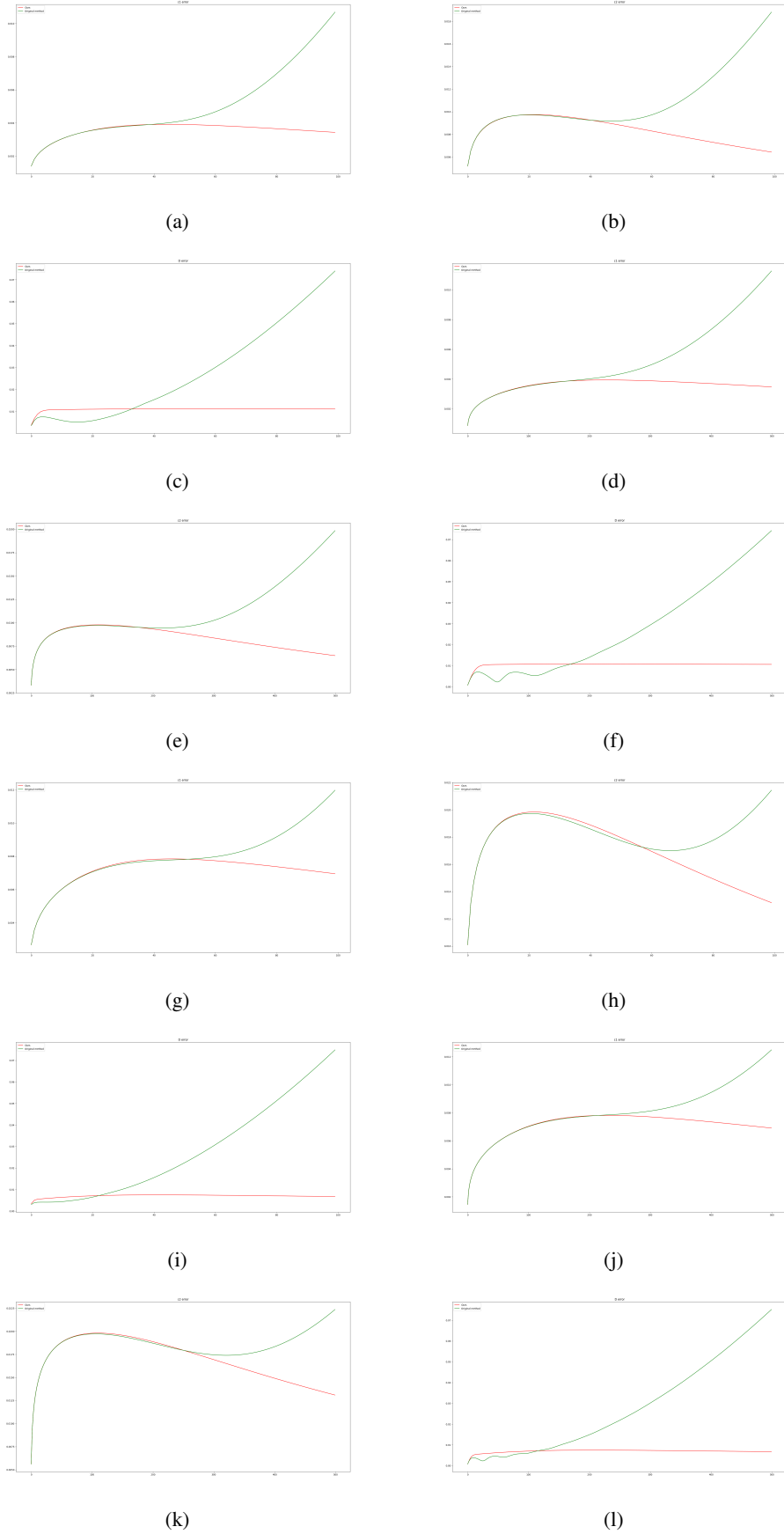
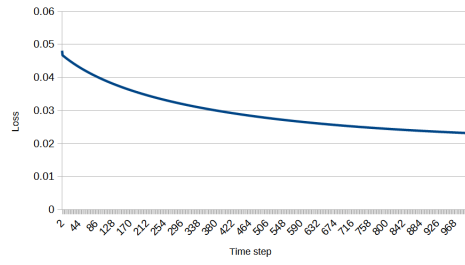


Figure 3: The error of  $c^1$ ,  $c^2$ , and  $D$  at the different time steps in different experiment settings. Red lines are ours, and green lines are that of the original method [32, 31]. (a)–(c)  $\Delta x = \Delta y = 0.02$ ,  $\Delta t = 0.005$ ; (d)–(f)  $\Delta x = \Delta y = 0.02$ ,  $\Delta t = 0.001$ ; (g)–(i)  $\Delta x = \Delta y = 0.04$ ,  $\Delta t = 0.005$ ; (j)–(l)  $\Delta x = \Delta y = 0.04$ ,  $\Delta t = 0.001$



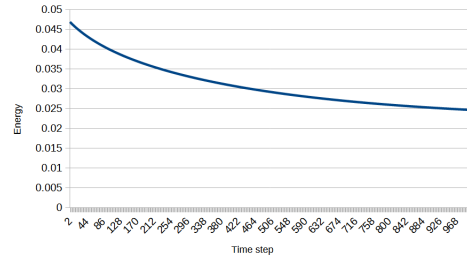


Figure 8: Free energy vs. time steps.

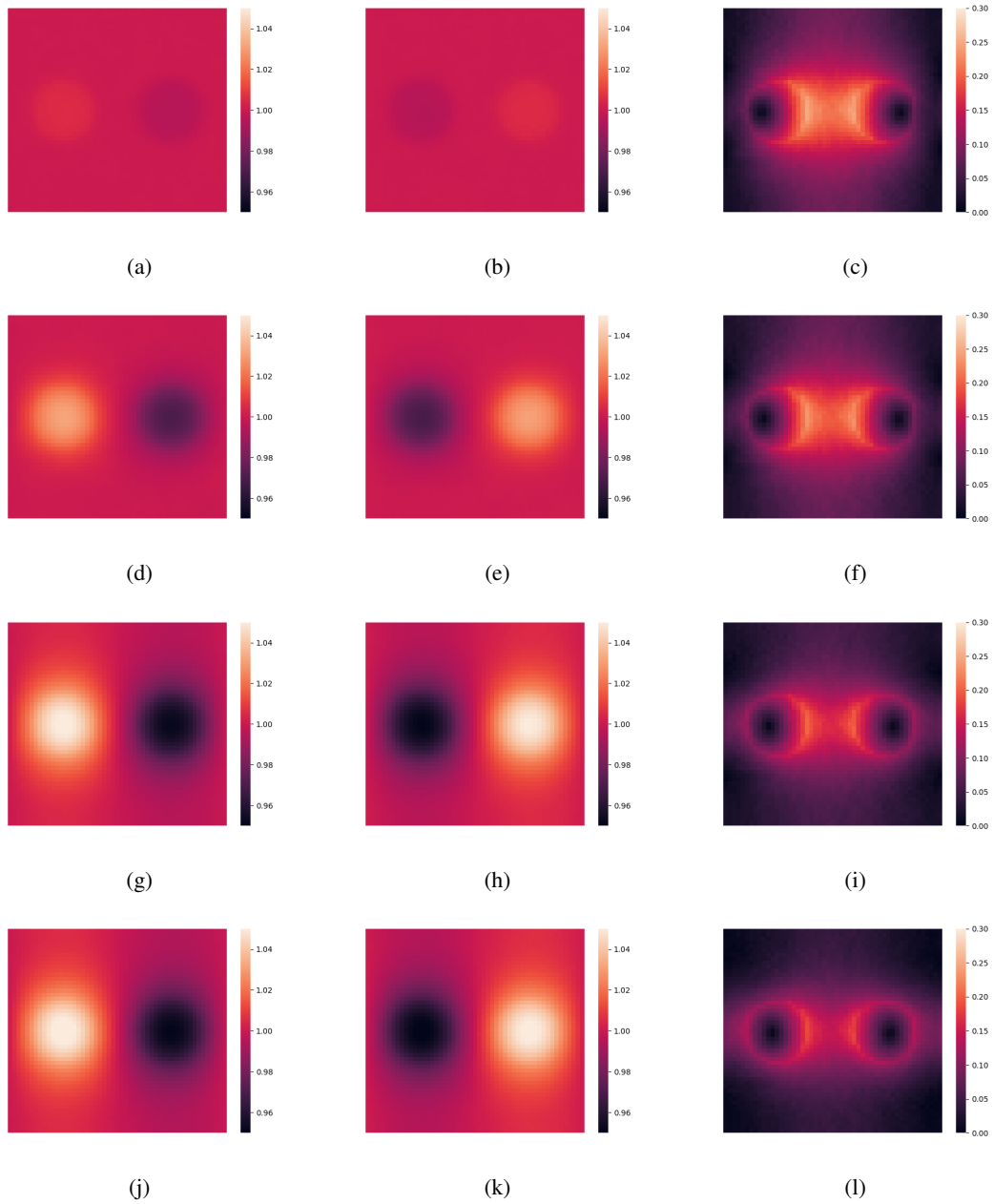


Figure 9:  $c^1$ ,  $c^2$ , and the  $l_2$ -norm of  $D$  at the different time steps. (a)–(c) Results at time step 10; (d)–(f) results at time step 100; (g)–(i) results at time step 500; (j)–(l) results at time step 1000

- [2] Dario Amodei, Sundaram Ananthanarayanan, Rishita Anubhai, Jingliang Bai, Eric Battenberg, Carl Case, Jared Casper, Bryan Catanzaro, Qiang Cheng, Guoliang Chen, Jie Chen, Jingdong Chen, Zhijie Chen, Mike Chrzanowski, Adam Coates, Greg Diamos, Ke Ding, Niandong Du, Erich Elsen, Jesse Engel, Weiwei Fang, Linxi Fan, Christopher Fougner, Liang Gao, Caixia Gong, Awni Hannun, Tony Han, Lappi Johannes, Bing Jiang, Cai Ju, Billy Jun, Patrick LeGresley, Libby Lin, Junjie Liu, Yang Liu, Weigao Li, Xiangang Li, Dongpeng Ma, Sharan Narang, Andrew Ng, Sherjil Ozair, Yiping Peng, Ryan Prenger, Sheng Qian, Zongfeng Quan, Jonathan Raiman, Vinay Rao, Sanjeev Satheesh, David Seetapun, Shubho Sengupta, Kavya Srinet, Anuroop Sriram, Haiyuan Tang, Liliang Tang, Chong Wang, Jidong Wang, Kaifu Wang, Yi Wang, Zhijian Wang, Zhiqian Wang, Shuang Wu, Likai Wei, Bo Xiao, Wen Xie, Yan Xie, Dani Yogatama, Bin Yuan, Jun Zhan, and Zhenyao Zhu. Deep speech 2 : End-to-end speech recognition in english and mandarin. In Maria Florina Balcan and Kilian Q. Weinberger, editors, *Proceedings of The 33rd International Conference on Machine Learning*, volume 48 of *Proceedings of Machine Learning Research*, pages 173–182, New York, New York, USA, 20–22 Jun 2016. PMLR.
- [3] Matt Gardner, Joel Grus, Mark Neumann, Oyvind Tafjord, Pradeep Dasigi, Nelson F. Liu, Matthew Peters, Michael Schmitz, and Luke Zettlemoyer. AllenNLP: A deep semantic natural language processing platform. In *Proceedings of Workshop for NLP Open Source Software (NLP-OSS)*, pages 1–6, Melbourne, Australia, July 2018. Association for Computational Linguistics.
- [4] M. W. M. G. Dissanayake and N. Phan-Thien. Neural-network-based approximations for solving partial differential equations. *Communications in Numerical Methods in Engineering*, 10(3):195–201, 1994.
- [5] I.E. Lagaris, A. Likas, and D.I. Fotiadis. Artificial neural networks for solving ordinary and partial differential equations. *IEEE Transactions on Neural Networks*, 9(5):987–1000, 1998.
- [6] Justin Sirignano and Konstantinos Spiliopoulos. Dgm: A deep learning algorithm for solving partial differential equations. *Journal of Computational Physics*, 375:1339–1364, 2018.
- [7] E. M. Wright. Adaptive control processes: a guided tour. by richard bellman. 1961. 42s. pp. xvi 255. (princeton university press). *The Mathematical Gazette*, 46(356):160–161, 1962.
- [8] E Weinan and Ting Yu. The deep ritz method: A deep learning-based numerical algorithm for solving variational problems. *Communications in Mathematics and Statistics*, 6:1–12, 2017.
- [9] M. Raissi, P. Perdikaris, and G.E. Karniadakis. Physics-informed neural networks: A deep learning framework for solving forward and inverse problems involving nonlinear partial differential equations. *Journal of Computational Physics*, 378:686 – 707, 2019.
- [10] Ameya D. Jagtap, Ehsan Kharazmi, and George Em Karniadakis. Conservative physics-informed neural networks on discrete domains for conservation laws: Applications to forward and inverse problems. *Computer Methods in Applied Mechanics and Engineering*, 365:113028, 2020.
- [11] Ehsan Kharazmi, Zhongqiang Zhang, and George Em Karniadakis. Variational physics-informed neural networks for solving partial differential equations. *CoRR*, abs/1912.00873, 2019.
- [12] Yaohua Zang, Gang Bao, Xiaojing Ye, and Haomin Zhou. Weak adversarial networks for high-dimensional partial differential equations. *Journal of Computational Physics*, 411:109409, 2020.
- [13] Ehsan Kharazmi, Zhongqiang Zhang, and George E.M. Karniadakis. hp-vpinns: Variational physics-informed neural networks with domain decomposition. *Computer Methods in Applied Mechanics and Engineering*, 374:113547, 2021.
- [14] Zhi-Qin John Xu, Yaoyu Zhang, Tao Luo, Yanyang Xiao, and Zheng Ma. Frequency principle: Fourier analysis sheds light on deep neural networks. *Communications in Computational Physics*, 28(5):1746–1767, 2020.
- [15] Stefano Markidis. The old and the new: Can physics-informed deep-learning replace traditional linear solvers? *Frontiers in Big Data*, 4, 2021.
- [16] Nils Margenberg, Dirk Hartmann, Christian Lessig, and Thomas Richter. A neural network multigrid solver for the navier-stokes equations. *Journal of Computational Physics*, 460:110983, 2022.
- [17] Charles C. Margossian. A review of automatic differentiation and its efficient implementation. *WIREs Data Mining and Knowledge Discovery*, 9(4):e1305, 2019.
- [18] Zhiwei Fang. A high-efficient hybrid physics-informed neural networks based on convolutional neural network. *IEEE Transactions on Neural Networks and Learning Systems*, pages 1–13, 2021.
- [19] Zixue Xiang, Wei Peng, Weien Zhou, and Wen Yao. Hybrid finite difference with the physics-informed neural network for solving pde in complex geometries, 2022.
- [20] Chunyue Lv, Lei Wang, and Chenming Xie. A hybrid physics-informed neural network for nonlinear partial differential equation. *International Journal of Modern Physics C*, 34(06):2350082, 2023.

- [21] Pao-Hsiung Chiu, Jian Cheng Wong, Chinchun Ooi, My Ha Dao, and Yew-Soon Ong. Can-pinn: A fast physics-informed neural network based on coupled-automatic-numerical differentiation method. *Computer Methods in Applied Mechanics and Engineering*, 395:114909, 2022.
- [22] Sebastian K. Mitusch, Simon W. Funke, and Miroslav Kuchta. Hybrid fem-nn models: Combining artificial neural networks with the finite element method. *Journal of Computational Physics*, 446:110651, 2021.
- [23] Haiyang He and Jay Pathak. An unsupervised learning approach to solving heat equations on chip based on auto encoder and image gradient. *CoRR*, abs/2007.09684, 2020.
- [24] Rishikesh Ranade, Chris Hill, and Jay Pathak. Discretizationnet: A machine-learning based solver for navier–stokes equations using finite volume discretization. *Computer Methods in Applied Mechanics and Engineering*, 378:113722, 2021.
- [25] Allen Flavell, Michael Machen, Bob Eisenberg, Julianne Kabre, Chun Liu, and Xiaofan Li. A conservative finite difference scheme for poisson–nernst–planck equations. *Journal of Computational Electronics*, 13(1):235–249, 2014.
- [26] Hailiang Liu and Zhongming Wang. A free energy satisfying finite difference method for poisson–nernst–planck equations. *Journal of Computational Physics*, 268:363–376, 2014.
- [27] Mohammad Mirzadeh and Frédéric Gibou. A conservative discretization of the poisson–nernst–planck equations on adaptive cartesian grids. *Journal of Computational Physics*, 274:633–653, 2014.
- [28] Pengzhan Jin, Zhen Zhang, Aiqing Zhu, Yifa Tang, and George Em Karniadakis. Sympnets: Intrinsic structure-preserving symplectic networks for identifying hamiltonian systems. *Neural Networks*, 132:166–179, 2020.
- [29] M. Mattheakis, P. Protopapas, D. Sondak, M. Di Giovanni, and E. Kaxiras. Physical symmetries embedded in neural networks. *arXiv paper*, (1904.08991), 2019.
- [30] Lee, Jae Yong, Jang, Jin Woo, and Hwang, Hyung Ju. The model reduction of the vlasov–poisson–fokker–planck system to the poisson–nernst–planck system via the deep neural network approach. *ESAIM: M2AN*, 55(5):1803–1846, 2021.
- [31] Zhonghua Qiao, Zhenli Xu, Qian Yin, and Shenggao Zhou. Structure-preserving numerical method for maxwell–ampère nernst-planck model. *Journal of Computational Physics*, 475:111845, 2023.
- [32] Zhonghua Qiao, Zhenli Xu, Qian Yin, and Shenggao Zhou. A maxwell–ampère nernst-planck framework for modeling charge dynamics, 2022.
- [33] A. C. Maggs and V. Rossetto. Local simulation algorithms for coulomb interactions. *Physical Review Letters*, 88(19), apr 2002.
- [34] J. Kiefer and Jacob Wolfowitz. Stochastic estimation of the maximum of a regression function. *Annals of Mathematical Statistics*, 23:462–466, 1952.
- [35] Diederik P. Kingma and Jimmy Ba. Adam: A method for stochastic optimization. *CoRR*, abs/1412.6980, 2014.
- [36] Xiaoxiao Guo, Wei Li, and Francesco Iorio. Convolutional neural networks for steady flow approximation. In *Proceedings of the 22nd ACM SIGKDD International Conference on Knowledge Discovery and Data Mining*, KDD ’16, page 481–490, New York, NY, USA, 2016. Association for Computing Machinery.
- [37] YUEHAW KHOO, JIANFENG LU, and LEXING YING. Solving parametric pde problems with artificial neural networks. *European Journal of Applied Mathematics*, 32(3):421–435, July 2020.
- [38] *Mathematical foundation of the stokes problem*, pages 1–57. Springer Berlin Heidelberg, Berlin, Heidelberg, 1979.
- [39] R.J. Plemmons. M-matrix characterizations.i—nonsingular m-matrices. *Linear Algebra and its Applications*, 18(2):175–188, 1977.
- [40] Chiun-Chang Lee, Hijin Lee, Yunkyong Hyon, Tai-Chia Lin, and Chun Liu. New poisson–boltzmann type equations: one-dimensional solutions. *Nonlinearity*, 24:431, 12 2010.
- [41] John R. Nickolls, Ian Buck, Michael Garland, and Kevin Skadron. Scalable parallel programming with cuda. *2008 IEEE Hot Chips 20 Symposium (HCS)*, pages 1–2, 2008.